

Nuclear Symmetry Energy and Neutron Skin Thickness of ^{208}Pb using a finite range simple effective interaction

D. Behera*, S. K. Tripathy†, T. R. Routray ‡and B. Behera§

The properties of nuclear matter at subsaturation densities can be probed from different isovector observables from finite nuclei. We use a finite range simple effective interaction to study the density dependence of nuclear symmetry energy and obtained a correlation between the neutron skin thickness in ^{208}Pb and the density slope parameter at a subsaturation density. A linear relation is obtained between the bulk part of the neutron skin thickness and the parameter $\frac{E'_s(\rho_c)}{E_s(\rho_0)}$ where $E_s(\rho_0)$ and $E'_s(\rho_c)$ are respectively the nuclear symmetry energy at saturation density and its first derivative at a subsaturation density.

PACS number: 21.65.Ef, 24.30.Cz

I. INTRODUCTION

The nuclear symmetry energy (NSE) $E_s(\rho)$ defined as the energy cost per particle for changing all the protons into neutrons in symmetric nuclear matter (SNM) is a fundamental quantity in nuclear physics and astrophysics. It provides a link to the properties of atomic nuclei with the structure and dynamics of neutron stars. An accurate knowledge of NSE is essential to understand the equation of state (EoS) of isospin asymmetric nuclear matter (ANM). In fact, the understanding and constraining the EoS of dense neutron-rich matter has remained a major goal in nuclear science research [1]. In neutron stars, NSE controls the proton fraction of the beta stable matter and decides the cooling mechanism and thickness of the neutron star crusts [2–4]. Also, $E_s(\rho)$ has a great role in obtaining the mass-radius relation and tidal deformability in neutron star [5]. In astrophysics, its behaviour is required to understand the supernova explosion mechanism and stellar nucleosynthesis [6–8]. In nuclear physics, NSE is a basic input for calculation of heavy-ion collision processes, prediction of properties of exotic nuclei with large neutron excess. Experimentally, $E_s(\rho)$ is not a directly measurable quantity and has to be extracted from isospin sensitive observables. The experimental determination of NSE therefore depends on the reliability of the model in describing the experimental observables. Although, it remains a quite challenging task, in the last one and half decade, a lot of theoretical and experimental efforts have been made to constrain the density dependence of NSE. In recent years, significant progress has been made to constrain the NSE at low densities from dynamical behaviour [9, 10], resonances and excitations [11–14], static properties of finite nuclei [15–18], neutron skin thickness [19–25] and electric dipole polarisability [14, 26–28]. The density dependence of $E_s(\rho)$ is largely unknown, except the value of $E_s(\rho)$ at saturation density to be around $32 \pm 4 \text{ MeV}$. However, the derivatives of the nuclear symmetry energy at saturation such as the density slope parameter $L(\rho_0)$ and curvature parameter $K_{\text{sym}}(\rho_0)$ are still uncertain. [29, 30]. Depending upon the observable and method of analysis, $L(\rho_0)$ varies significantly from 20 MeV to 115 MeV [14]. The reason behind this uncertainty lies in the fact that, the task of extracting of these isovector quantities from experimental data is not that easy. One needs to assume some models and than the data of stable nuclei to the parameters of the assumed models are fitted. This process may not constrain the isovector part of the nuclear equation of states in a precise way [20].

Neutron skin thickness (NST) has proved to be a better tool to improve our knowledge in the isovector channels of nuclear effective interaction [31–35]. The Lead Radius Experiment (PREX) is able to determine the neutron radius in ^{208}Pb upto 1% accuracy through the measurement of the parity violating asymmetry at low momentum transfer in the polarised elastic electron scattering performed at a single angle [36]. This experiment provides the first purely electroweak, model-independent measurement of the weak charge form factor which is closely related to the neutron skin thickness of ^{208}Pb . A measurement of the form factor of ^{208}Pb at a momentum transfer of $q \simeq 0.475 \text{ fm}^{-1}$, yielded the PREX results $\Delta r_{np} = 0.33^{+0.16}_{-0.18} \text{ fm}$ [36]. The nuclear droplet model (DM) [37] suggested that NST in heavy nucleus is related to different symmetry energy parameters. On the basis of DM, it has been predicted from different mean field models in ^{208}Pb that, NST is linearly correlated with the density slope parameter [39]. In recent years, different correlation systematics of isovector properties of finite nuclei with NST have yielded constraints on

* 1. Department of Physics, Indira Gandhi Institute of Technology, Sarang, Dhenkanal, Odisha-759146, India

2. School of Physics, Sambalpur University, Jyotivihar, Sambalpur, Odisha-768019, India, E-mail:dipadolly@rediffmail.com

† Department of Physics, Indira Gandhi Institute of Technology, Sarang, Dhenkanal, Odisha-759146, India, E-mail:tripathy_sunil@rediffmail.com

‡ Retired Professor, School of Physics, Sambalpur University, Jyotivihar, Sambalpur, Odisha-768019, India, E-mail:trr1@rediffmail.com

§ Retired Professor, School of Physics, Sambalpur University, Jyotivihar, Sambalpur, Odisha-768019, India

the density slope parameter and the curvature symmetry parameter [19–21, 38, 39]. However so far a consensus has not yet been reached in this direction.

The purpose of the present work is two fold. First, we construct nuclear equations of state using a finite range simple effective interaction so that it reproduces the basic features of SNM at saturation density and the nuclear symmetry energy at the subsaturation cross density $\rho_c = 0.11 \text{ fm}^{-3}$ as constrained in a recent work from analysing the binding energy difference of heavy isotope pairs[23]. Similar method has been adopted in a recent work [40] to constrain the density dependence of NSE at high density. The EoS constructed in this procedure is employed to study the density dependence of NSE. Second, through a comprehensive and quantitative analysis, we correlate the neutron skin thickness and the energy constant of Isovector giant dipole resonance (IVGDR) of ^{208}Pb to the isovector indicators of the finite range effective interaction. The paper is organised as follow: in Section II, the basic formalism of the finite range effective interaction and the method of parameter fixation are discussed. The constructed EoSs are used to investigate the density dependence of NSE. In Section III, we discuss the mass dependence of symmetry energy coefficient of finite nuclei. In Section IV, we carried out a comprehensive analysis for the correlation of the neutron skin thickness with the density slope parameter at saturation density and at a reference density ρ_c . The correlation of IVGDR of ^{208}Pb with the isovector indicators of the effective interaction is also presented. At the end the conclusion and summary are presented in Section-V.

II. MODEL AND METHOD

A. Nuclear Symmetry Energy and Nuclear Equation of state

For an isospin asymmetric nuclear matter (ANM) with neutron-proton asymmetry δ , neutron density ρ_n , proton density ρ_p , the energy per nucleon $e(\rho, \delta)$ can be written as

$$e(\rho, \delta) = \frac{1}{\pi^2 \rho} [f(k_n) + f(k_p)] + V(\rho, \delta), \quad (1)$$

where $\rho = \rho_n + \rho_p$ is the nucleon density, $k_{n,p}$ are the neutron(proton) Fermi momenta. $V(\rho, \delta)$ is the interaction part of the equation of state, $e(\rho, \delta)$. The kinetic part of the EoS is treated in the relativistic Fermi gas model and the functional $f(k_i)$ with $i = n, p$ is expressed as

$$f(k_i) = \int_0^{k_f} (c^2 \hbar^2 k^2 + M^2 c^4)^{\frac{1}{2}} k^2 dk. \quad (2)$$

Here, Mc^2 is the rest mass of the nucleon. The interaction part of $e(\rho, \delta)$ has a complicated dependence on ρ and δ because of the presence of finite range exchange interaction between nucleons. However, the isospin exchange symmetry allows us to expand the EoS in even powers of the neutron-proton asymmetry δ as

$$e(\rho, \delta) = e_0(\rho) + E_s(\rho)\delta^2 + \mathcal{O}(\delta^4), \quad (3)$$

where $e_0(\rho) = e(\rho, \delta = 0)$ is the energy per particle in symmetric nuclear matter (SNM). $E_s(\rho)$ is nuclear symmetry energy defined as

$$E_s(\rho) = \frac{1}{2!} \frac{\partial^2 e(\rho, \delta)}{\partial \delta^2} \Big|_{\delta=0}. \quad (4)$$

Assuming that the contribution from higher order terms in δ is small, the NSE can be expressed as the difference in the energy per particle in pure neutron matter $e_n(\rho) = e(\rho, \delta = 1)$ and that in SNM,

$$E_s(\rho) = e_n(\rho) - e_0(\rho). \quad (5)$$

An expansion of $E_s(\rho)$ around the saturation density ρ_0 reads as

$$E_s(\rho) = E_s(\rho_0) + \frac{L}{3} \left(\frac{\rho - \rho_0}{\rho_0} \right) + \frac{K_{sym}}{18} \left(\frac{\rho - \rho_0}{\rho_0} \right)^2 + \dots, \quad (6)$$

where $L(\rho_0) = 3\rho_0 \frac{\partial E_s(\rho)}{\partial \rho} \Big|_{\rho=\rho_0}$ and $K_{sym} = 9\rho_0^2 \frac{\partial^2 E_s(\rho)}{\partial \rho^2} \Big|_{\rho=\rho_0}$ are the slope and curvature parameters of $E_s(\rho)$ at ρ_0 . Upto 2nd order in density, the density dependence of NSE depends on the parameters $L(\rho_0)$ and $K_{sym}(\rho_0)$.

B. Finite range effective interaction

In the present work, we consider a finite range simple effective interaction (SEI)

$$v_{eff}(\mathbf{r}) = t_0(1 + x_0 P_\sigma) \delta(\mathbf{r}) + \frac{1}{6} t_3 (1 + x_3 P_\sigma) \left[\frac{\rho(\mathbf{R})}{1 + b\rho(\mathbf{R})} \right]^\gamma \delta(\mathbf{r}) + (W + BP_\sigma - HP_\tau - MP_\sigma P_\tau) f(r), \quad (7)$$

where $f(r)$ represents a finite range Yukawa interaction $\frac{e^{-r/\alpha}}{r/\alpha}$. Here α is the range of the interaction. \mathbf{r} and \mathbf{R} are respectively the relative and centre of mass coordinates of the two interacting nucleons. W, B, H and M are the strength of the Wigner, Bartlett, Heisenberg and Majorana components. P_σ and P_τ are the spin and isospin exchange operators respectively. The simple effective interaction is similar to the Skyrme type interaction except the fact that the t_1 and t_2 terms of the Skyrme interaction are replaced by a finite range term. Also, the t_3 term has been modified. The replacement of the t_1 and t_2 terms by a finite range term is essential to account for the correct momentum dependence of the nuclear mean field as extracted from the optical model fits in heavy-ion collision studies at intermediate energies [41–48]. In the denominator of the t_3 term we have considered a factor $(1 + b\rho(\mathbf{R}))^\gamma$ to avoid the supra luminous behaviour of the nuclear matter equation of state at high density region. The simple effective interaction contains altogether 11 adjustable parameters namely $t_0, x_0, t_3, x_3, b, \gamma, W, B, H, M$ and α . This SEI has already been used to study the momentum and density dependence of the isoscalar part of the nuclear mean field at zero and finite temperature [49–51], isovector part of the nuclear mean field at zero temperature [52], temperature dependence of nuclear symmetry energy [53, 54]. The SEI has also been used to calculate the half-lives of spherical proton emitters [55].

The energy density $H(\rho, y_p, T)$ in ANM at a density ρ , proton fraction y_p and temperature T can be obtained from SEI as

$$\begin{aligned} H(\rho, y_p, T) = & \int [f_T^n(\mathbf{k}) + f_T^p(\mathbf{k})] (c^2 \hbar^2 k^2 + M^2 c^4) d^3 k \\ & + \frac{1}{2} \left[\frac{\varepsilon_0^l}{\rho_0} + \frac{\varepsilon_\gamma^l}{\rho_0^{\gamma+1}} \left(\frac{\rho}{1 + b\rho} \right)^\gamma \right] (\rho_n^2 + \rho_p^2) + \left[\frac{\varepsilon_0^{ul}}{\rho_0} + \frac{\varepsilon_\gamma^{ul}}{\rho_0^{\gamma+1}} \left(\frac{\rho}{1 + b\rho} \right)^\gamma \right] \rho_n \rho_p \\ & + \frac{\varepsilon_{ex}^l}{2\rho_0} \int \int [f_T^n(\mathbf{k}) f_T^n(\mathbf{k}') + f_T^p(\mathbf{k}) f_T^p(\mathbf{k}') g_{ex}(|\mathbf{k} - \mathbf{k}'|)] d^3 k d^3 k' \\ & + \frac{\varepsilon_{ex}^{ul}}{2\rho_0} \int \int [f_T^n(\mathbf{k}) f_T^p(\mathbf{k}') + f_T^p(\mathbf{k}) f_T^n(\mathbf{k}') g_{ex}(|\mathbf{k} - \mathbf{k}'|)] d^3 k d^3 k', \end{aligned} \quad (8)$$

where $f_T^\tau(\mathbf{k})$, $\tau = n, p$ are the respective Fermi-Dirac distribution functions and $g_{ex}(|\mathbf{k} - \mathbf{k}'|) = \frac{1}{1 + \frac{|\mathbf{k} - \mathbf{k}'|^2}{\Lambda^2}}$. Λ is inversely related to the range parameter i.e. $\Lambda = \frac{1}{\alpha}$. The study of ANM involves nine parameters: $\gamma, b, \varepsilon_0^l, \varepsilon_0^{ul}, \varepsilon_\gamma^l, \varepsilon_\gamma^{ul}, \varepsilon_{ex}^l, \varepsilon_{ex}^{ul}$ and the range parameter α . The parameters $\varepsilon_0^l, \varepsilon_0^{ul}, \varepsilon_\gamma^l, \varepsilon_\gamma^{ul}, \varepsilon_{ex}^l, \varepsilon_{ex}^{ul}$ are related to the parameters of SEI [56].

The energy per particle in symmetric nuclear matter at zero temperature ($T = 0$) for the Yukawa type simple finite range interaction becomes

$$e_0(\rho) = \frac{3Mc^2}{8x_f^3} [2x_f u_f^3 - x_f u_f - \ln(x_f + u_f)] + \frac{\varepsilon_0}{2} \frac{\rho}{\rho_0} + \frac{\varepsilon_\gamma}{2} \frac{\rho}{\rho_0^{\gamma+1}} \left(\frac{\rho}{1 + b\rho} \right)^\gamma + \frac{\varepsilon_{ex}}{2\rho_0} \rho J_0(\rho), \quad (9)$$

where $x_f = \frac{\hbar k_f}{Mc}$, $u_f = (1 + x_f)^{\frac{1}{2}}$ and $k_f = (1.5\pi^2 \rho)^{\frac{1}{3}}$ is the Fermi momentum in SNM. The functional $J_0(\rho)$ is given by

$$J_0(\rho) = \frac{\int \left(\frac{3j_1(k_f r)}{k_f r} \right)^2 \frac{e^{-r/\alpha}}{r/\alpha} d^3 r}{\int \frac{e^{-r/\alpha}}{r/\alpha} d^3 r}. \quad (10)$$

Here $j_1(k_f r)$ is the first order spherical Bessel function and $\varepsilon_0 = \frac{1}{2} (\varepsilon_0^l + \varepsilon_0^{ul})$, $\varepsilon_\gamma = \frac{1}{2} (\varepsilon_\gamma^l + \varepsilon_\gamma^{ul})$, $\varepsilon_{ex} = \frac{1}{2} (\varepsilon_{ex}^l + \varepsilon_{ex}^{ul})$.

The energy per particle in pure neutron matter (PNM) at zero temperature is obtained from the SEI as

$$e_n(\rho) = \frac{3Mc^2}{8x_n^3} [2x_n u_n^3 - x_n u_n - \ln(x_n + u_n)] + \frac{\varepsilon_0^l}{2} \frac{\rho}{\rho_0} + \frac{\varepsilon_\gamma^l}{2} \frac{\rho}{\rho_0^{\gamma+1}} \left(\frac{\rho}{1 + b\rho} \right)^\gamma + \frac{\varepsilon_{ex}^l}{2\rho_0} \rho J_n(\rho), \quad (11)$$

where $x_n = \frac{\hbar k_n}{Mc}$, $u_n = (1 + x_n)^{\frac{1}{2}}$ and $k_n = (3\pi^2 \rho)^{\frac{1}{3}}$ is the Fermi momentum in PNM. The functional $J_n(\rho)$ is given by

$$J_n(\rho) = \frac{\int \left(\frac{3j_1(k_n r)}{k_n r} \right)^2 \frac{e^{-r/\alpha}}{r/\alpha} d^3 r}{\int \frac{e^{-r/\alpha}}{r/\alpha} d^3 r}. \quad (12)$$

TABLE I: Values of the interaction parameters in SNM.

Parameters in SNM	γ	b (fm^3)	α (fm)	ε_0 (MeV)	ε_γ (MeV)	ε_{ex} (MeV)
	0.5	0.5668	0.4044	-57.86	76.91	-121.84

TABLE II: Values of the interaction parameters in PNM.

Parameter sets in PNM	$E_s(\rho_0)$ (MeV)	$E_s(\rho_c)$ (MeV)	$E'_s(\rho_0)$ (MeV)	$K_{sym}(\rho_0)$ (MeV)	$E_s(2\rho_0)$ (MeV)	ε_0^l (MeV)	ε_γ^l (MeV)	ε_{ex}^l (MeV)
Set I	33	26.65	14.72	-201.32	38.65	-1.7401	21.0099	-81.2299
Set II	34	26.65	18.35	-168.86	44.76	-11.2489	33.0473	-81.2299
Set III	35	26.65	22	-136.16	50.90	-20.8451	45.1762	-81.2299

C. Constraining the interaction parameters

The complete description of SNM requires only the knowledge of six parameters $\gamma, b, \alpha, \varepsilon_0, \varepsilon_\gamma$ and ε_{ex} . However, the equation of state in PNM requires the splitting of the strength parameters $\varepsilon_0, \varepsilon_\gamma$ and ε_{ex} into like (l) and unlike (ul) channels. The parameters α and ε_{ex} are obtained from a simultaneous optimization procedure so as to provide a correct momentum and density dependence of the nuclear mean field in SNM as demanded by the optical model fits to the heavy-ion collision data at intermediate energies. During the optimization procedure, it is kept in view that, the nuclear mean field in SNM at saturation density vanishes for a kinetic energy of $300 MeV/n$. ε_0 and ε_γ are determined from the saturation condition in normal nuclear matter. Here we have used the fact that, $Mc^2 = 939 MeV$, energy per nucleon in SNM $e_0(\rho_0) = 923 MeV$, $\left(c^2\hbar^2k_{f_0}^2 + M^2c^4\right)^{\frac{1}{2}} = 976 MeV$ and the saturation density $\rho_0 = 0.1658 fm^{-3}$. The stiffness of the equation of state in SNM determines the exponent γ . In the present work, we have used $\gamma = \frac{1}{2}$ corresponding to the incompressibility in normal nuclear matter $K = 240 MeV$. The parameters as constrained from different physical basis to determine the EoS of SNM are given in Table I.

There are no experimental or empirical constraints on the splitting of $\varepsilon_0, \varepsilon_\gamma$ and ε_{ex} into the corresponding like (l) and unlike (ul) components. However, from an analysis of the entropy density in PNM and SNM, ε_{ex}^l has been constrained in a recent work as $\varepsilon_{ex}^l = \frac{2}{3}\varepsilon_{ex}$ [53]. For this constrained value of ε_{ex}^l , the neutron effective mass in neutron-rich matter is predicted to pass over the proton effective mass. Eventhough, controversy prevails among the results from different theoretical models about the neutron-proton effective mass splitting, there is almost a consensus reached on the fact that, neutron effective mass in neutron rich matter will go over the proton effective mass. For a given splitting of ε_{ex} into ε_{ex}^l and ε_{ex}^{ul} , the splitting of other two strength parameters ε_0 and ε_γ into like and unlike components requires the knowledge of the zero temperature nuclear symmetry energy $E_s(\rho_0)$ and its slope $E'_s(\rho_0) = \rho \frac{dE_s(\rho)}{d\rho}|_{\rho=\rho_0} = \frac{1}{3}L(\rho_0)$ at saturation density. During the last one or two decades, there have been a lot of experimental and theoretical efforts to constrain these parameters. However, amidst all these efforts, still there exist uncertainties in the values of $E_s(\rho_0)$ and $L(\rho_0)$ [3, 10, 57–61]. While the $E_s(\rho_0)$ is constrained to a narrow range of $E_s(\rho_0) = 32 \pm 4 MeV$, there is a large uncertainty in the values of $L(\rho_0)$. Different theoretical models predict similar $E_s(\rho)$ at saturation density but widely differ in the values of $L(\rho_0)$ and therefore predict quite different density dependence of NSE. The slope parameter has been constrained recently in the range $L(\rho_0) = 41.6 \pm 7.6 MeV$ from Lublin-Stasbourg nuclear drop energy (LSD) formula [62]. Constraints on the NSE have been obtained in recent times from the properties of finite nuclei such as the nuclear binding energy [29, 63, 64], neutron skin thickness [12, 20, 21, 33, 65–67], electric response (dipole polarisability)[14]. Properties of finite nuclei provide stringent constraints on $E_s(\rho)$ and $L(\rho)$ at subsaturation densities. From an analysis of the binding energy difference of heavy isotope pairs, Zhang and Chen have obtained a tighter constraint on the symmetry energy at subsaturation density $\rho_c = 0.11 fm^{-3}$ i.e. $E_s(\rho_c) = 26.65 \pm 0.20 MeV$ [23]. It is worth to mention here that, the average density of heavy nuclei such as ^{208}Pb is around $0.11 fm^{-3}$. On the other hand, density dependence of NSE at high density is quite uncertain. However there have been a significant progress in understanding the high density behaviour of NSE from terrestrial nuclear laboratories and astrophysical observations. The upper limit of tidal deformability for canonical neutron stars $\Lambda_{1.4} = 580$ extracted from GW170817 by LIGO and VIRGO collaborators [68] has allowed to constrain the high density nuclear equation of state to a narrow range. From the analysis of these observations for a constant maximum mass of $M_{max} = 2.01M_\odot$ and radius $R_{1.4} = 12.83$, the high density behaviour of NSE has been constrained at a density $\rho = 2\rho_0$ to be $E_s(2\rho_0) = 46.9 \pm 10.1 MeV$ [69, 70]. Using the extracted upper limit on the tidal deformability of the gravitational waves from GW170817, Tong et al. have also obtained a constraint on the NSE at twice saturation density as $E_s(2\rho_0) \leq 60.7 \pm 10.9 MeV$ [71]. Bayesian analysis of the radii of canonical Neutron Stars predicts $E_s(2\rho_0) = 39.2^{+12.1}_{-8.2} MeV$ [72]. Zhang et al. constrained the NSE from an analysis of heavy ion collision data, neutron skin of ^{208}Pb , tidal deformability and maximum mass of neutron stars obtained $E_s(2\rho_0)$ in the range $35 - 55 MeV$ [73]. In order to constrain our interaction parameters so as to provide a good description of the nuclear symmetry density both at a subsaturation cross density as well as at a reasonably high density (as

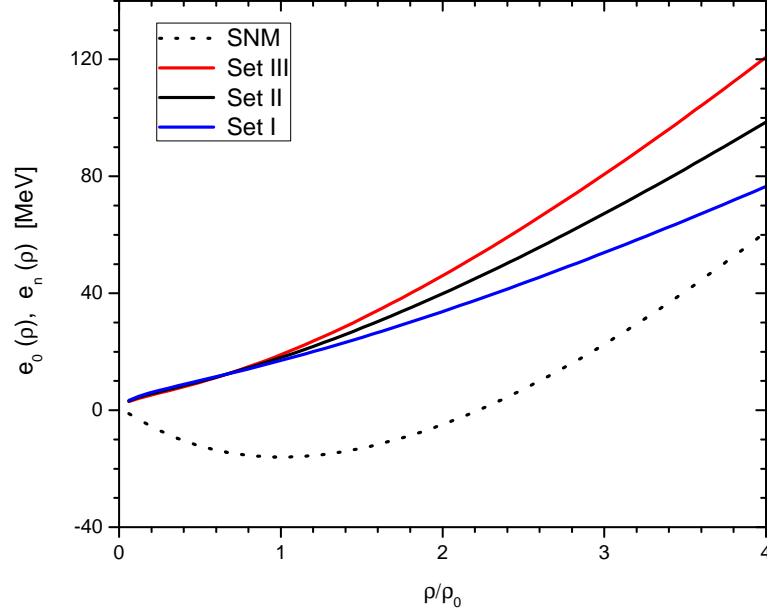


FIG. 1: Energy per particle in SNM and PNM for three different parameter sets of the finite range simple effective interaction. The dotted curve is for SNM and the solid curves represent the energy per particle in PNM.

applicable to neutron stars), in the present work, we have varied the slope parameter for a given $E_s(\rho_0)$ within its acceptable range to obtain the $E_s(\rho_c) = 26.65 \pm 0.2 \text{ fm}^{-3}$. The slope parameter that fixes the constrained $E_s(\rho_c)$ are then checked so as to predict the NSE at $2\rho_0$ close to the limit $E_s(2\rho_0) = 46.9 \pm 10.1 \text{ MeV}$. In this procedure, we obtained the splitting of the strength parameters ε_0 and ε_γ into like and unlike components. We have considered three different values of $E_s(\rho_0)$ namely $E_s(\rho_0) = 33, 34$ and 35 MeV and obtained the corresponding splitted parameter sets. The parameters of the given finite range SEI as constrained above for the EoS of PNM are given in Table II. The slope parameter for all the sets lie in the acceptable range $44 \leq L(\rho_0) \leq 66 \text{ MeV}$. In the table, we have also given the $K_{sym}(\rho_0)$ values as predicted from the constructed equation of states. For all the sets of nuclear equation of state, the values of $K_{sym}(\rho_0)$ lie in the range $-201 \leq K_{sym}(\rho_0) \leq -126 \text{ MeV}$. The NSE at $2\rho_0$ lie in the range $38.65 \leq E_s(2\rho_0) \leq 52.15 \text{ MeV}$. These values are well within those predicted from terrestrial and astrophysical observations [69, 70, 73]. For completeness, we have shown the EoSs for SNM and PNM for the three different parameter sets of the finite range effective interaction in Figure 1.

D. Density dependence of Nuclear Symmetry Energy

In Figure 2, we have shown the density dependence of the NSE for three different sets of parameters. Also, we have plotted the NSE as obtained from a comparison of FOPI-LAND data concerning the elliptic-flow ratio of neutrons with respect to charged particles with ultra relativistic quantum molecular dynamics (UrQMD) transport model [74]. In that study Russotto et al. have used parametrized form of NSE

$$E_s(\rho)[\text{MeV}] = 12 \left(\frac{\rho}{\rho_0} \right)^{2/3} + 22 \left(\frac{\rho}{\rho_0} \right)^\gamma, \quad (13)$$

and constrained the exponent as $\gamma = 0.72 \pm 0.19$ [74]. This is an improvement over a similar study that suggested a moderately soft to linear NSE characterised by an exponent $\gamma = 0.9 \pm 0.4$ [75]. These studies have ruled out supersoft scenarios for NSE. In Fig. 2, we have also included the behaviour of NSE at subnormal densities as obtained from different studies [9, 60]. Our constructed sets of NSE are quite compatible with these results at low density region. However, in the high density region beyond the normal nuclear matter density, our results for the sets with $E_s(\rho_0) = 33$ and 34 MeV pass below the predicted results from the UrQMD study of FOPI-LAND data [74]. Only the set with $E_s(\rho_0) = 35 \text{ MeV}$ passes through the shaded region (refer to Fig. 2) and therefore may comprise a more suitable equation of state for neutron-rich asymmetric nuclear matter. At normal nuclear matter density, our NSE for set III goes above the FOPI-LAND data because of the fact that, in the parametrized form used in Ref.[74] has a sharp value of $E_s(\rho_0) = 34 \text{ MeV}$. Regarding the density dependence behaviour the NSE for the other two sets can not simply be ruled out on the basis of the FOPI-LAND data. Recently, Zhou and Chen [40], on the basis of the

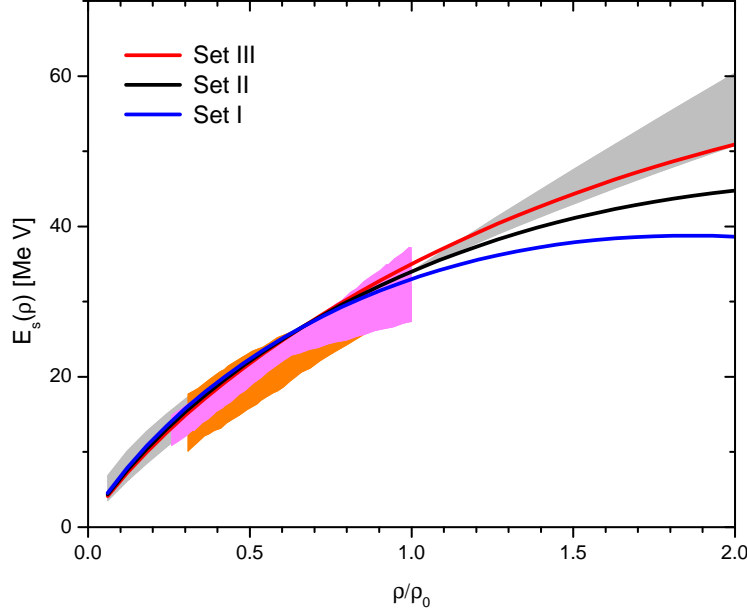


FIG. 2: Nuclear symmetry energy $E_s(\rho)$ as a function of the reduced density $\frac{\rho}{\rho_0}$. The results at subnormal densities of Ref.[9, 60] and the UrQMD results (shaded grey region) of FOPI-LAND data of Ref. [74] are also shown in the figure. The shaded region in orange is for the HIC results of Sn+Sn reaction and the pink region is for the results of IAS.

discovery of millisecond PSR J0740+6620 with Mass $2.14^{+0.10}_{-0.09} M_\odot$ [76] together with the data of finite nuclei ruled out super soft NSE that becomes negative at suprasaturation densities in neutron stars. On that basis, the set II with $E_s(\rho_0) = 34 \text{ MeV}$ will pass the test. The set I with $E_s(\rho_0) = 33 \text{ MeV}$ can be viable according to the constraints of Refs. [69, 70].

In order to understand the density dependence of NSE as calculated from the finite range SEI, we can split it into its kinetic contribution and the contribution from the interaction part

$$E_s(\rho) = E_s^{kin}(\rho) + E_s^{pot}(\rho), \quad (14)$$

where

$$E_s^{kin}(\rho) = \frac{3Mc^2}{8} \left[\frac{2x_n u_n^3 - x_n u_f - \ln(x_n + u_n)}{x_n^3} - \frac{2x_f u_f^3 - x_f u_n - \ln(x_f + u_f)}{x_f^3} \right], \quad (15)$$

and

$$E_s^{pot}(\rho) = \frac{(\varepsilon_0^l - \varepsilon_0)}{2} \frac{\rho}{\rho_0} + \frac{(\varepsilon_\gamma^l - \varepsilon_\gamma)}{2} \frac{\rho}{\rho_0^{\gamma+1}} \left(\frac{\rho}{1 + b\rho} \right)^\gamma + \frac{[\varepsilon_{ex}^l J_n(\rho) - \varepsilon_{ex} J_0(\rho)]}{2} \frac{\rho}{\rho_0}. \quad (16)$$

In Figure 3, the kinetic and potential contributions to the NSE are shown as function of the reduced nuclear density $\frac{\rho}{\rho_0}$. It is obvious that, the kinetic part has a positive contribution behaving as $\left(\frac{\rho}{\rho_0}\right)^{2/3}$. But the potential contribution depends on the value of $E_s(\rho_0)$ and $L(\rho_0)$. For a given pair of $E_s(\rho_0)$ and $L(\rho_0)$, the potential part $E_s^{pot}(\rho)$ increases to attain a peak and then decreases with an increase in the reduced nuclear density. The peak value and the corresponding reduced density $\left(\frac{\rho}{\rho_0}\right)_{max}$ increase with the increase in the values of $E_s(\rho_0)$ and $L(\rho_0)$. Consequently, the $E_s^{pot}(\rho)$ with low values of $E_s(\rho_0)$ and $L(\rho_0)$ quickly becomes negative and thereby makes the NSE soft or supersoft. Since the exchange strength parameters ε_{ex} and ε_{ex}^l are fixed for all the sets, the contribution coming from the exchange term remains the same. In fact, this exchange contribution to NSE increases with an increase in the nuclear matter density. One can note that, the contribution from the term involving the parameters ε_0 and ε_0^l is positive and the contribution from the term involving the parameters ε_γ and ε_γ^l is negative. This negative contribution decreases as we increase the $E_s(\rho_0)$ value. Consequently, the potential contribution to NSE becomes more and more negative after certain nuclear matter density leading to a softer NSE.

The slope parameter $L(\rho_0) = 3E'_s(\rho_0)$ as obtained from the fitting procedure can be correlated with the $E_s(\rho_0)$. In fact these two parameters decide the density dependence of NSE and are highly correlated. From different mean field

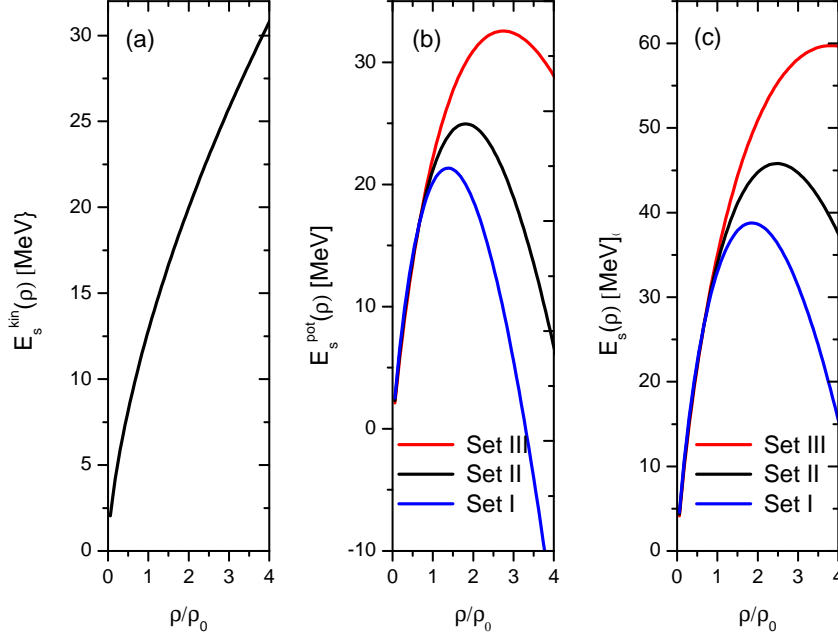


FIG. 3: Components of Nuclear symmetry energy $E_s(\rho)$ as a function of the reduced density $\frac{\rho}{\rho_0}$. In the extreme left panel we have shown the kinetic energy contribution to the NSE. In the middle panel, the contribution coming from the interaction part is shown and in the right panel, the total NSE is plotted.

models, it is found that, these two parameters are linearly correlated. Roca-Maza et al. have obtained a correlation between $E_s(\rho_0)$ and $L(\rho_0)$ from the experimentally measured values $19.6 \pm 0.6 \text{ fm}^3$ of the dipole polarisability of ^{208}Pb as $E_s(\rho_0) = (24.5 \pm 0.8) + (0.168 \pm 0.007)L(\rho_0)$ [65]. Lattimer and Steiner [77] have obtained a similar but slightly different correlation relation from the experimental value of the dipole polarisability of ^{208}Pb as reported by Tamii et al. [12]. In Figure 4, we have shown these experimentally extracted correlation of $E_s(\rho_0)$ and $L(\rho_0)$. The shaded region in grey in the figure represents the correlation of Roca-Maza et al. and the region between the two blue lines represents the correlation of Lattimer and Steiner. In the figure we have also shown the correlation from IAS results as extracted from Ref. [77]. The red dots are the results of the present work as constrained from the fitting procedure of the interaction parameter of the finite range simple effective interaction. At a given $E_s(\rho_0)$, we have obtained three different values of $L(\rho_0)$ corresponding to the fitting of the NSE to the value of $E_s(\rho_c) = 26.65 \pm 0.2 \text{ MeV}$. The correlation between $E_s(\rho_0)$ and $L(\rho_0)$ from our calculations are more or less similar and compatible to that of Roca-Maza et al. It may be noted from the figure that all the points of our calculation lie in the grey shaded region even though the results corresponding to $E_s(\rho_0) = 35 \text{ MeV}$ overlap with the region extracted by Lattimer and Steiner.

In order to have an idea of the behaviour of the symmetry energy at a reference density $\rho_c < \rho_0$, we may expand the NSE around $E_s(\rho_c)$ as

$$E_s(\rho) = E_s(\rho_c) + L(\rho_c)\varepsilon + \frac{K_{sym}(\rho_c)}{2!}\varepsilon^2 + \mathcal{O}(\varepsilon^3), \quad (17)$$

where $\varepsilon = \frac{\rho - \rho_c}{3\rho_c}$. $L(\rho_c) = 3\rho_c \frac{dE_s(\rho)}{d\rho}|_{\rho=\rho_c}$ is the density slope parameter and $K_{sym}(\rho_c) = 9\rho_c^2 \frac{d^2E_s(\rho)}{d\rho^2}|_{\rho=\rho_c}$ is the curvature parameter at the reference density ρ_c . Knowledge of $L(\rho_c)$ besides being an important quantity in determining the density dependence of the NSE at low density region, plays an important role in determining the neutron skin thickness of heavy nuclei. In view of this, more precise constraints on $L(\rho_c)$ will help a lot in the understanding of the nuclear equation of state. We have plotted the NSE as a function of the parameter ε in Figure 5 for the three sets assuming the reference density as the central density for ^{208}Pb . In the figure, the NSE of Russotto et al. [74] with a parametrized form as in Eq.(13) and the extracted value of the exponent as $\gamma = 0.72$ is also shown for comparison. The values of the parameters $L(\rho_c)$ and $K_{sym}(\rho_c)$ have also been calculated from the expression of the NSE. Both the extracted values along with the calculated values of $L(\rho_c)$ and $K_{sym}(\rho_c)$ are given in the Table III. Recently Zhang and Chen [14] have extracted the value of $L(\rho_c)$ from the analysis of the electric dipole polarisability in ^{208}Pb as $L(\rho_c) = 47.3 \pm 7.8$. From the present calculations, the $L(\rho_c)$ are predicted to be $46.69 \leq L(\rho_c) \leq 55.63 \text{ MeV}$ which are well within the extracted values of Zhang and Chen [14]. Using the finite range simple effective interaction, we have obtained $K_{sym}(\rho_c)$ in the range $-120.69 \leq K_{sym}(\rho_c) \leq -82.8 \text{ MeV}$. It is worth to mention here that, while empirical constraints on $L(\rho_c)$ are available in literature there are no such constraints on the parameter $K_{sym}(\rho_c)$.

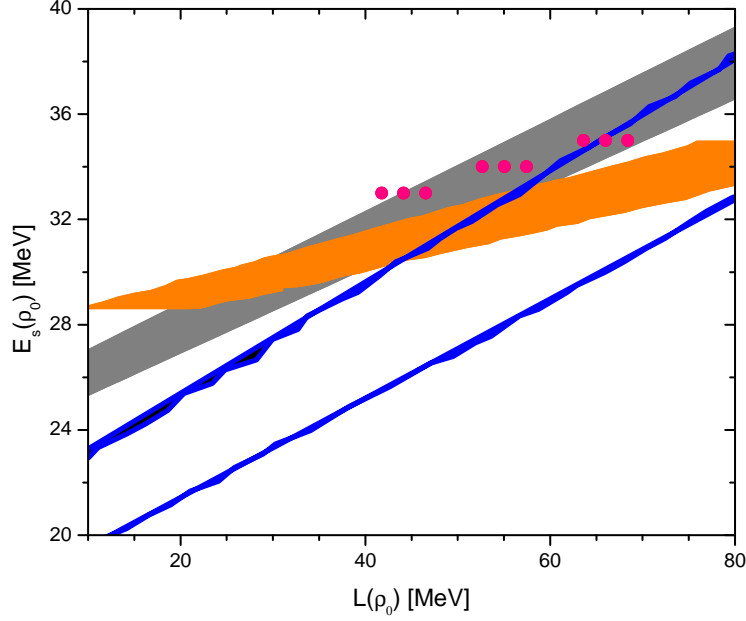


FIG. 4: Nuclear symmetry energy $E_s(\rho)$ as a function of $L(\rho_0)$ as extracted from different works. The grey region represents the results of Roca-Maza et al. [65]. The region between the two thick blue lines represent the results of Lattimer and Steiner [77]. The orange region is the correlation from IAS results as extracted from Ref.[77]. The red dots are the calculated values from the present work.

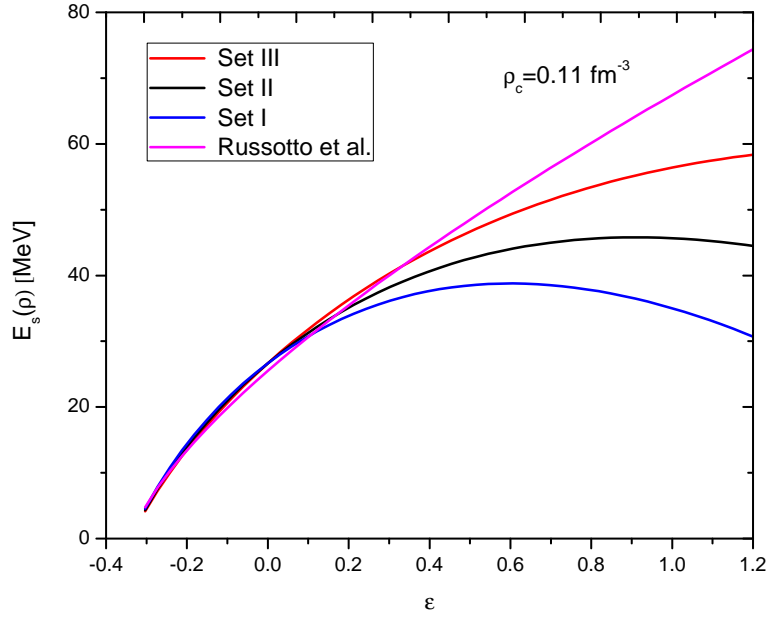


FIG. 5: Nuclear symmetry energy $E_s(\rho)$ as a function of $\varepsilon = \frac{\rho - \rho_c}{3\rho_c}$. The results of Ref. [74] are also shown in the figure for comparison.

III. SYMMETRY ENERGY COEFFICIENT

To understand the behaviour of nuclear symmetry energy in nuclear masses, it is essential to have a correlation of the symmetry energy coefficient in finite nuclei $a_{sym}(A)$ and the NSE $E_s(\rho)$. Within the droplet model (DM), Centelles et al. [19, 78] have found that the symmetry energy coefficient $a_{sym}(A)$ of finite nuclei with mass number A is equal to the nuclear symmetry energy, $E_s(\rho_A)$ calculated at the central density ρ_A of the nucleus i.e $a_{sym}(A) \simeq E_s(\rho_A)$.

TABLE III: Prediction of different isovector indicators from the finite range effective interaction.

Parameter sets	$L(\rho_0)$ (MeV)	$L(\rho_c)$ (MeV)	$K_{sym}(\rho_c)$ (MeV)	a_{ss} (MeV)	a_{cs} (MeV)	Q (MeV)
Set I	44.16	46.69	-120.69	43.88	36.46	52.59
Set II	55.05	51.15	-101.82	52.44	51.17	46.81
Set III	66.0	55.63	-82.80	61.05	65.97	42.42

They have shown that, this relation not only works for heavy nuclei such as ^{208}Pb but also holds for medium mass nuclei [78]. Such a relation is helpful in providing a direct correlation of the isospin observables of finite nuclei with $E_s(\rho)$ at subnormal densities.

The symmetry energy coefficient $a_{sym}(A)$ in finite nuclei can also be expressed as [78]

$$a_{sym}(A) = \frac{E_s(\rho_0)}{1 + x_A}, \quad (18)$$

where

$$x_A = \frac{9}{4} \frac{E_s(\rho_0)}{Q} A^{-1/3}. \quad (19)$$

Q is the surface stiffness parameter that measures the resistance of the nucleus against separation of neutrons from protons to form a skin. This quantity is directly related to the nuclear surface symmetry energy [37, 64]. Usually Q is obtained from semi-infinite nuclear matter calculations [79, 80]. The surface stiffness parameter can be calculated from the expression [81, 82]

$$Q = \frac{9}{4} \left(L(\rho_0) - \frac{K_{sym}(\rho_0)}{12} \right)^{-1} E_s^2(\rho_0). \quad (20)$$

However, in the present work, we have used the expression

$$Q = \frac{9}{4} \left(\frac{E_s(\rho_0)}{a_{sym}(A)} - 1 \right)^{-1} E_s(\rho_0) A^{-1/3}. \quad (21)$$

The calculated values of the surface stiffness coefficient are given in Table III. One can note that, with an increase in the values of $L(\rho_0)$ and $E_s(\rho_0)$, the value of Q decreases.

Assuming the relation $a_{sym}(A) \simeq E_s(\rho)$ to be valid in a wide range of nuclear mass, we have calculated the symmetry energy coefficient for the three sets of nuclear EoSs. For this purpose we have used the density parametrization

$$\rho_A = \frac{\rho_0}{1 + \kappa A^{-1/3}}, \quad (22)$$

where the constant κ is fixed to reproduce the density of ^{208}Pb . In Figure 6, the reference density ρ_A as calculated from Eq. (22) is shown as a function of mass number A . The reference density of heavy nuclei are usually considered in literature as close to 0.1 fm^{-3} . The same has been reflected in the figure. The reference density increases with A and almost saturates for large nuclear masses. In Figure 7, the symmetry energy coefficient of finite nuclei is plotted as a function of the mass number for the three different sets of interaction parameters. In the plot, we have extrapolated the results to large values of nuclear mass $A = 1000$ to get an idea of the asymptotic value of $a_{sym}(A)$. As the mass number increases, $a_{sym}(A)$ increases slowly to reach its asymptotic value. In the figure, we have also shown the $a_{sym}(A)$ as calculated by using SLy4 interaction [83, 84]. Even though the behaviour of the curve for SLy4 is the same as that of the curves for finite range SEI, it lies below the SEI curves. The reason may lie in the fact that, the finite range interaction parameters are fitted in such a manner to reproduce the empirically constrained value of $E_s(\rho_c) = 26.65 \pm 0.2 \text{ MeV}$ for ^{208}Pb [23] whereas for the SLy4 interaction $a_{sym}(208)$ is around 22.90 MeV . It can be observed that, the three sets namely Set I, Set II and Set III predict almost similar values for $a_{sym}(A)$ with a little spread both at the high mass and low mass region.

In a leptodermous expansion within liquid drop model, the symmetry energy coefficient can be expanded in powers of $A^{-1/3}$ as

$$a_{sym}(A) = E_s(\rho_0) - a_{ss} A^{-1/3} + a_{cs} A^{-2/3}, \quad (23)$$

where a_{ss} is the coefficient of the surface symmetry term and a_{cs} is the coefficient of the curvature symmetry term. We have fitted the $a_{sym}(A)$ as calculated from Set I, Set II and Set III to Eq.(23) and extracted the coefficients a_{ss} and a_{cs} . The values of these coefficients are given in Table III. One can note that, the values of a_{ss} and a_{cs} increase with an increase in the value of $L(\rho_c)$.

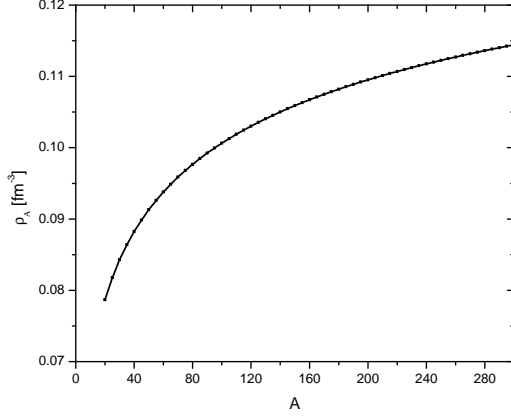


FIG. 6: Reference density ρ_A as a function of mass number A . The reference density for ^{208}Pb is taken as 0.11 fm^{-3} .

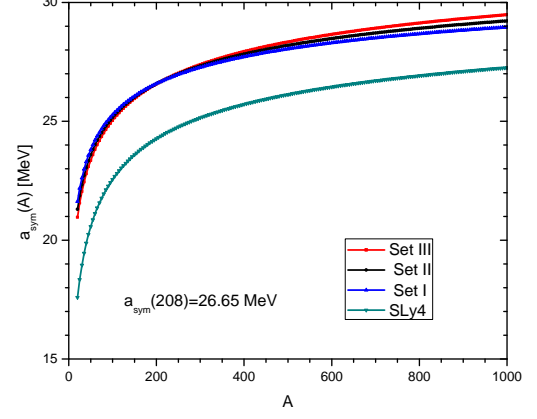


FIG. 7: Symmetry energy coefficient $a_{sym}(A)$ as a function of mass number A for the three EoSs. The results of SLy4 interaction [83] are also shown in the graph for comparison.

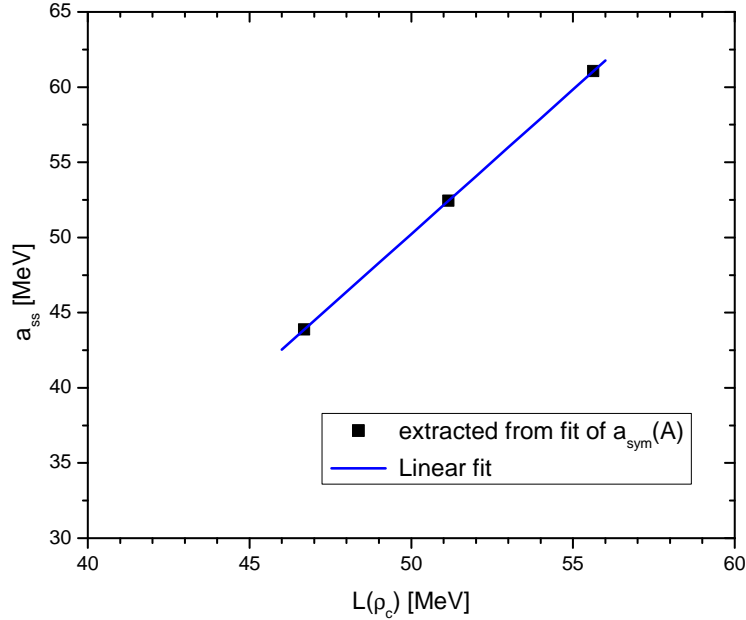


FIG. 8: Surface symmetry coefficient a_{ss} as extracted from leptodermous expansion of $a_{sym}(A)$ as a function of the density slope parameter $L(\rho_c)$ at reference density. Here the $L(\rho_c)$ values are considered for ^{208}Pb as given Table III. The plot also shows a linear fit between a_{ss} and $L(\rho_c)$.

Keeping upto first order in $A^{-1/3}$ in Eq. (23), we can express the surface symmetry term as

$$a_{ss} = [E_s(\rho_0) - a_{sym}(A)] A^{1/3}. \quad (24)$$

Substituting for $a_{sym}(A)$ from Eq.(17) in Eq. (23), we obtain

$$a_{ss} = [E_s(\rho_0) - E_s(\rho_c) - L(\rho_c)\varepsilon] A^{1/3}. \quad (25)$$

Here the relation $a_{sym}(A) \simeq E_s(\rho)$ is assumed and the expansion in Eq.(17) is truncated after first order term in ε . This equation (25) clearly indicates a linear relation between the surface symmetry term and the density slope parameter at a reference density. In Figure 8, we have shown the linear correlation between the extracted a_{ss} and $L(\rho_c)$. A linear fit of the data points provides the relationship

$$a_{ss} = -45.872 + 1.922L(\rho_c). \quad (26)$$

IV. NEUTRON SKIN THICKNESS OF ^{208}Pb

The neutron skin thickness (NST) is defined as the difference between the rms radii for the density distribution of the neutrons and protons in the nucleus,

$$\Delta r_{np} = \langle r^2 \rangle_n^{1/2} - \langle r^2 \rangle_p^{1/2}, \quad (27)$$

which can be expressed as [21]

$$\Delta r_{np} = \Delta r_{np}^{bulk} + \Delta r_{np}^{Coul} + \Delta r_{np}^{surf}. \quad (28)$$

The bulk part $\Delta r_{np}^{bulk} = \sqrt{\frac{3}{5}}(R_n - R_p)$ is proportional to the distance between the neutron and proton radii of uniform sharp distributions. $\Delta r_{np}^{Coul} = -\sqrt{\frac{3}{5}}\frac{e^2 Z}{70 E_s(\rho_0)}$ is a correction due to the Coulomb repulsion and $\Delta r_{np}^{surf} = 2.5\sqrt{\frac{3}{5}}\left(\frac{b_n^2}{R_n} - \frac{b_p^2}{R_p}\right) \simeq \sqrt{\frac{3}{5}}\frac{5}{2R}(b_n^2 - b_p^2)$ is a correction due to the difference in the surface widths b_n and b_p of the neutron and proton profiles.

It is well known that, the liquid drop model provides a useful tool to correlate the NST with different NSE parameters. In the present section, we wish to find out the correlations among the neutron skin thickness of ^{208}Pb and different isovector parameters of nuclear symmetry energy. Within the purview of DM [37] and neglecting the shell correction, the bulk part of NST can be expressed as

$$\Delta r_{np}^{bulk} = \sqrt{\frac{3}{5}}t, \quad (29)$$

where

$$t = \frac{3}{2}r_0 \frac{E_s(\rho_0)}{Q} \left(\frac{I - I_c}{1 + x_A} \right). \quad (30)$$

Here $R = r_0 A^{1/3}$, $r_0 = \left(\frac{4}{3}\pi\rho_0\right)^{-1/3}$ and $I_c = \frac{e^2 Z}{20 E_s(\rho_0) R}$ is the Coulomb correction to the symmetry energy coefficient.

Substituting the expressions of x_A from Eq. (18) and Q from Eq. (21) into the above relation (30), we obtain,

$$t = \frac{2}{3}r_0 \left[1 - \frac{a_{sym}(A)}{E_s(\rho_0)} \right] A^{1/3} (I - I_c). \quad (31)$$

Using Eq.(6) and $a_{sym}(A) = E_s(\rho_A)$, Eq.(31) can be reduced to

$$t \simeq -2r_0 \epsilon_A \beta \left(1 + \frac{K_{sym}(\rho_0)}{2L(\rho_0)} \epsilon_A \right) A^{1/3} (I - I_c), \quad (32)$$

where $\beta = \frac{L(\rho_0)/3}{E_s(\rho_0)} = \frac{E'_s(\rho_0)}{E_s(\rho_0)}$ and $\epsilon_A = \frac{\rho_c - \rho_0}{\rho_0}$. Obviously, Eqs.(31) and (32) suggest a correlation between the bulk part of the NST in finite nuclei and some isovector indicators such as $1 - \frac{a_{sym}(A)}{E_s(\rho_0)}$, β and $\frac{K_{sym}(\rho_0)}{E_s(\rho_0)}$. The close correlations among different isovector observables in finite nuclei with symmetry energy parameters have been studied in literature [13, 19–21, 23, 38, 39, 65, 78, 85, 86]. In most of the studies, the correlation between Δr_{np} or its bulk part of a given nucleus with $E_s(\rho_0)/Q$ or $L(\rho_0)$ have been performed. In some cases, Δr_{np} has been correlated with $E_s(\rho_0) - a_{sym}(A)$. The bulk part of NST or more specifically the quantity t , has a dominant contribution to the neutron skin thickness and depends on the nuclear symmetry energy parameters. Basing upon the expressions of t in Eqs. (31) and (32), it is more reasonable to correlate t with the isovector indicators such as $1 - \frac{a_{sym}(A)}{E_s(\rho_0)}$, β and $\frac{K_{sym}(\rho_0)}{E_s(\rho_0)}$. In the present work, we have considered three different values of $E_s(\rho_0)$ namely 33, 34 and 35 MeV and constrained the EoSs so as to reproduce the symmetry energy for ^{208}Pb in the range 26.65 ± 0.2 MeV. In view of this, in the correlation plots, we have considered the combined parameter $1 - \frac{a_{sym}(A)}{E_s(\rho_0)}$ taking into account the role of $E_s(\rho_0)$. In Figure 9, we plot Δr_{np} for ^{208}Pb as a function of $1 - \frac{a_{sym}(A)}{E_s(\rho_0)}$. In Figure 10, we show the correlation of the quantity t with $1 - \frac{a_{sym}(A)}{E_s(\rho_0)}$. In these figures, the results of the all the nine EoSs are shown. The shaded bands in the figures depict the prediction from the regression procedure. The respective Pearson correlation coefficients C_P are mentioned in the figures. One may note that, the Pearson correlation coefficient for Fig. 9 is 0.9995 and that for Fig. 10 is 0.99996. In otherwords, the correlation for the bulk part of the NST is much better as compared to that of the whole of the neutron skin thickness.

One should note that the quantity t is directly proportional to the parameter $\beta = \frac{E'_s(\rho_0)}{E_s(\rho_0)}$. Another fact is that, EoSs with same value of NSE at saturation density may have different slopes. In view of this, we emphasize the correlation between Δr_{np} and β instead of finding a compact relation between Δr_{np} and $L(\rho_0)$. For the EoSs employed in this

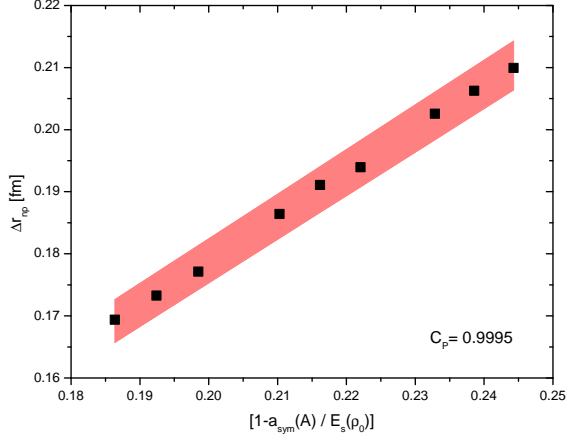


FIG. 9: The neutron skin thickness in ^{208}Pb is plotted as a function of the quantity $1 - \frac{a_{\text{sym}}(A)}{E_s(\rho_0)}$. The shaded region shows the correlation band with a Pearson correlation coefficient $C_P = 0.9995$.

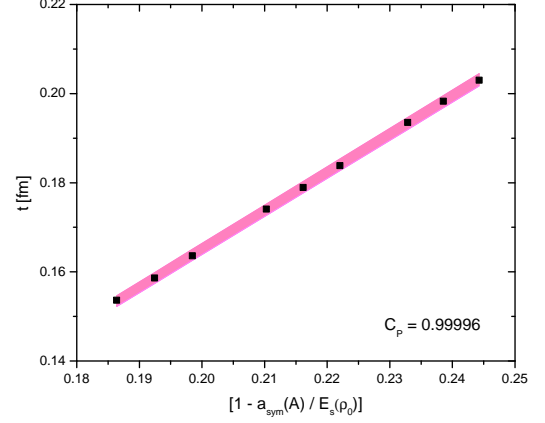


FIG. 10: The quantity t for ^{208}Pb is plotted as a function of the quantity $1 - \frac{a_{\text{sym}}(A)}{E_s(\rho_0)}$. The shaded region shows the correlation band with a Pearson correlation coefficient $C_P = 0.99996$.

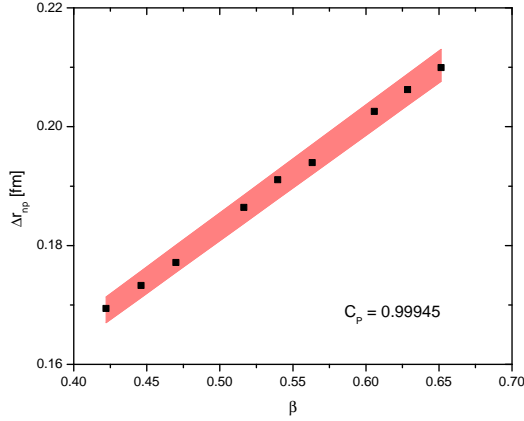


FIG. 11: The neutron skin thickness in ^{208}Pb is plotted as a function of the quantity β . The shaded region shows the correlation band with a Pearson correlation coefficient $C_P = 0.99945$.

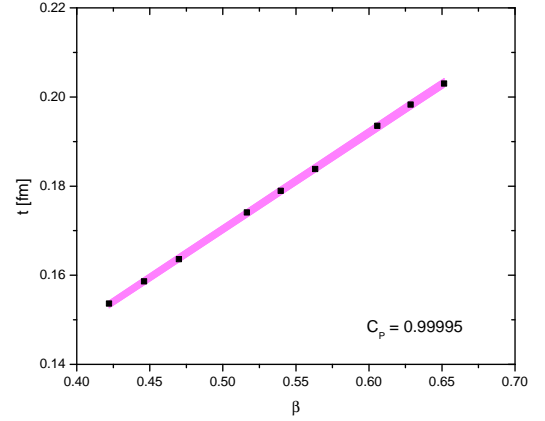


FIG. 12: The quantity t for ^{208}Pb is plotted as a function of the quantity β . The shaded region shows the correlation band with a Pearson correlation coefficient $C_P = 0.99995$.

work, Δr_{np} is calculated to be in the range $0.17 - 0.21 \text{ fm}$ for the range of $0.425 \leq \beta \leq 0.675$ with a spreading of around 0.04 fm . In Figures 11 and 12, we have shown respectively the correlation of Δr_{np} and t with the parameter β . It is interesting to note that, these quantities are highly correlated in a linear relationship. From a linear fit to the plots, we obtain the relationships

$$\Delta r_{np} = (0.0934 \pm 0.0012) + (0.1796 \pm 0.0023)\beta \text{ [fm]}, \quad (33)$$

$$t = (0.6196 \pm 0.0005) + (0.2167 \pm 0.0008)\beta \text{ [fm]}. \quad (34)$$

The values of Δr_{np} as estimated from the above relationship are in conformity with the predictions from a large sets of relativistic and non relativistic nuclear mean field models [13]. Usually $L(\rho_0)$ shows a linear relationship with the NST of finite nuclei. Roca-Maza et al. have extracted a linear relationship among Δr_{np} and $L(\rho_0)$ for ^{208}Pb as $\Delta r_{np} = 0.101 + 0.00147L(\rho_0)$ [39]. Substituting the values of $L(\rho_0)$ in this extracted relation from our work we obtain the NST in the range $0.16 \leq \Delta r_{np} \leq 0.2 \text{ fm}$. For a completeness, we have plotted the Δr_{np} as a function of $L(\rho_0)$ in Figure 13 and compared our results with that Ref. [39]. Results of some mean field calculations are also shown in the figure for comparison. The correlation coefficient in this case is $C_P = 0.99943$ a bit less than that of the $\Delta r_{np} \sim \beta$ plot. A linear fit of the results returns us the relation $\Delta r_{np} = (0.1066 \pm 0.00107) + (0.0015 \pm 0.000019)L(\rho_0)$. This expression predicts a bit higher value of the NST as compared to that of Roca-Maza et al.[39].

We next explore the correlation between the NST and the density slope parameter at a reference density ρ_c . Replacing ρ in by ρ_0 Eq. (17), we get

$$\frac{E_s(\rho_0) - a_{\text{sym}}(A)}{3E_s(\rho_0)} = \beta' \varepsilon \left[1 + \frac{1}{2} \frac{K_{\text{sym}}(\rho_c)}{L(\rho_c)} \varepsilon \right], \quad (35)$$

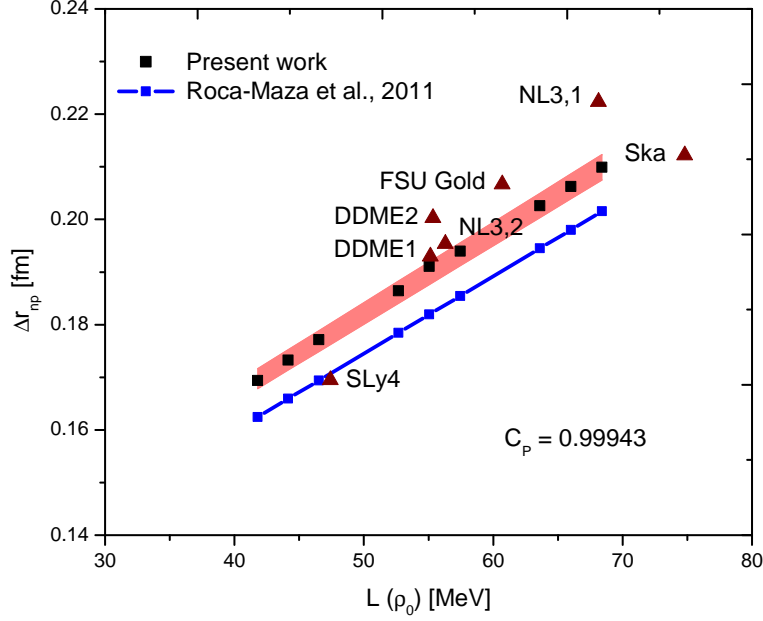


FIG. 13: The neutron skin thickness in ^{208}Pb is plotted as a function of the density slope parameter at saturation density. The solid triangles are the extracted results of some of the mean field calculations of Ref.[39]. The results are compared with the linear fit of the neutron skin thickness in ^{208}Pb with the density slope parameter as obtained in Ref. [39].

so that the distance between the neutron and proton mean surface locations becomes

$$t = 2r_0\varepsilon\beta' \left[1 + \frac{1}{2} \frac{K_{\text{sym}}(\rho_c)}{L(\rho_c)} \varepsilon \right] A^{1/3} (I - I_c), \quad (36)$$

where $\beta' = \frac{L(\rho_c)}{3E_s(\rho_0)}$ and the present value of ε is $\frac{\rho_0 - \rho_c}{3\rho_c}$. Eq. (36) suggests a correlation between the NST with the parameters β' and $K_{\text{sym}}(\rho_c)$. The correlation of the NST with β' and $K_{\text{sym}}(\rho_c)$ for the results of finite range simple effective interaction are shown in Figures 14 and 15. As expected these quantities are highly correlated as depicted by the respective correlation coefficients. Linear fits to the correlations provide the relationships

$$\Delta r_{np} = (-0.09263 \pm 0.00319) + (0.56413 \pm 0.00637)\beta' fm, \quad (37)$$

and

$$\Delta r_{np} = (0.27682 \pm 0.0025) + (0.00085 \pm 0.00002)K_{\text{sym}}(\rho_c) fm. \quad (38)$$

It is worth to mention here that, Δr_{np} shows a strong correlation among certain isovector observables of heavy finite nuclei such as ^{208}Pb . Therefore accurate determination of the NST of ^{208}Pb from experiments would provide constraints on the density dependence of NSE and on the slope parameter. The Lead Radius Experiment (PREX) [36] is able to determine the neutron radius in ^{208}Pb upto 1% accuracy through the measurement of the parity violating asymmetry at low momentum transfer. The PREX results for the neutron skin thickness in ^{208}Pb are $\Delta r_{np} = 0.33^{+0.16}_{-0.18} fm$ [36]. Experiments with hadronic probes constrained the NST in ^{208}Pb as $\Delta r_{np} = 0.16 \pm (0.02)_{\text{(stat)}} \pm (0.04)_{\text{(syst)}} fm$ [33] and $\Delta r_{np} = 0.211^{+0.054}_{-0.063}$ [34]. Measurement from coherent pion photoproduction yield a value $\Delta r_{np}(^{208}\text{Pb}) = 0.15 \pm 0.03 fm$ [87]. Our results from the finite range simple effective interactions are in conformity with these experimental results.

A. Correlation with Isovector Giant Dipole Resonance

Correlation with different collective excitation modes such as the Isovector Giant Dipole Resonance (IVGDR) may also put some constraints on the density dependence of the nuclear symmetry energy [88]. The IVGDR energy constant is expressed as

$$D = \sqrt{\frac{8\hbar^2}{mr_0^2} \left[\frac{E_s(\rho_0)}{1 + 3 \frac{E_s(\rho_0)}{Q} A^{-1/3}} \right]}. \quad (39)$$

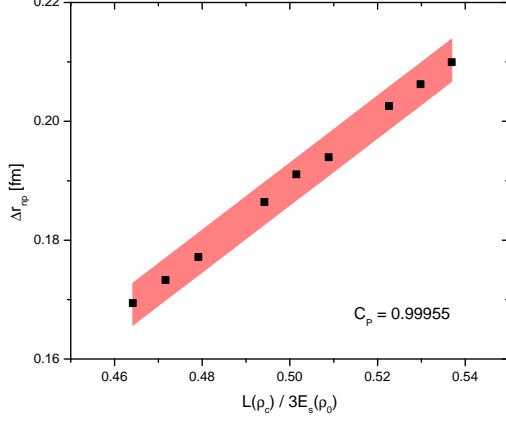


FIG. 14: Neutron skin thickness in ^{208}Pb is correlated with the quantity $\frac{L(\rho_c)}{3E_s(\rho_0)}$. The shaded region shows the correlation band with a Pearson correlation coefficient $C_P = 0.99955$.

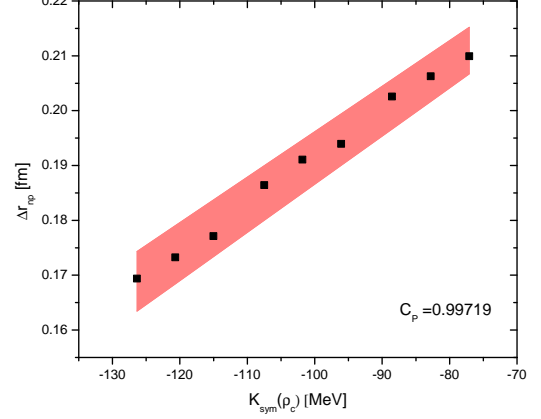


FIG. 15: Neutron skin thickness in ^{208}Pb is correlated with the quantity $K_{\text{sym}}(\rho_c)$. The shaded region shows the correlation band with a Pearson correlation coefficient $C_P = 0.99719$.

The IVGDR energy constant depends on the factor $E_s(\rho_0)/Q$ and consequently depends on the neutron skin thickness Δr_{np} . In the left panel of Figure 16, we have shown the IVGDR energy as a function of the neutron skin thickness. In the figure, we have shown the results of Ref. [85] for different Skyrme functional for comparison. The data points for the Skyrme functional remain below the data points of the present calculation. It is clear from the figure that there is a poor correlation between these two quantities. However, D appears to decrease with Δr_{np} . Since the NST depends on the density slope parameter at a reference density, it is expected that, D will have certain relation with $L(\rho_c)$. In the right panel of Figure 16, the IVGDR energy is plotted as a function of $L(\rho_c)$ obtained from the finite range simple effective interactions. It appears that D decreases with an increase in the value of $L(\rho_c)$.

We can write Eq. (39) as

$$D = \sqrt{\frac{8\hbar^2}{mr_0^2}} \left(\frac{3}{A^{1/3}Q} \right)^{-1/2} \left[1 + \frac{A^{1/3}Q}{3E_s(\rho_0)} \right]^{-1/2}. \quad (40)$$

Expanding the square-bracketed term in powers of $\frac{A^{1/3}Q}{3E_s(\rho_0)}$ and retaining upto the 1st order we get

$$D \simeq \sqrt{\frac{8\hbar^2}{mr_0^2}} \left(\frac{3}{A^{1/3}Q} \right)^{-1/2} \left[1 - \frac{A^{1/3}Q}{6E_s(\rho_0)} \right], \quad (41)$$

which may be expressed as

$$D = B_A \left(\frac{a_{\text{sym}}(A)}{t} \right)^{1/2} \left[1 - \frac{A^{1/3}Q}{6E_s(\rho_0)} \right]. \quad (42)$$

Here we have substituted the expression for Q from the relationship of t and defined a constant $B_A = \sqrt{\frac{4\hbar^2}{mr_0^2}} A^{1/3}(I - I_c)$ for a given nucleus. In Eq.(42), the leading term is proportional to $\left(\frac{a_{\text{sym}}(A)}{t} \right)^{1/2}$. This expression in Eq.(42) allows us to draw a linear correlation between the IVGDR energy and the quantity $\left(\frac{a_{\text{sym}}(A)}{t} \right)^{1/2}$.

In Figure 17, we have shown D as a function of $\left(\frac{a_{\text{sym}}(A)}{t} \right)^{1/2}$. As expected, the correlation between these quantities is better than the previous correlation between D and Δr_{np} . The Pearson correlation coefficient for the present case is $C_P = 0.82$. In the figure we have shown a linear fit to the correlated data points.

V. CONCLUSION

In the present work, we have studied the density dependence of nuclear symmetry energy using a finite range simple effective interaction. The effective interaction has a finite range part so as to describe the correct momentum dependence of the nuclear mean field as extracted from the optical model fits in the heavy-ion collision studies at intermediate energies. By exploring the recently constrained nuclear symmetry energy at a subsaturation cross density, we have constructed three different sets of nuclear EoSs from the SEI. The EoSs constructed in the present

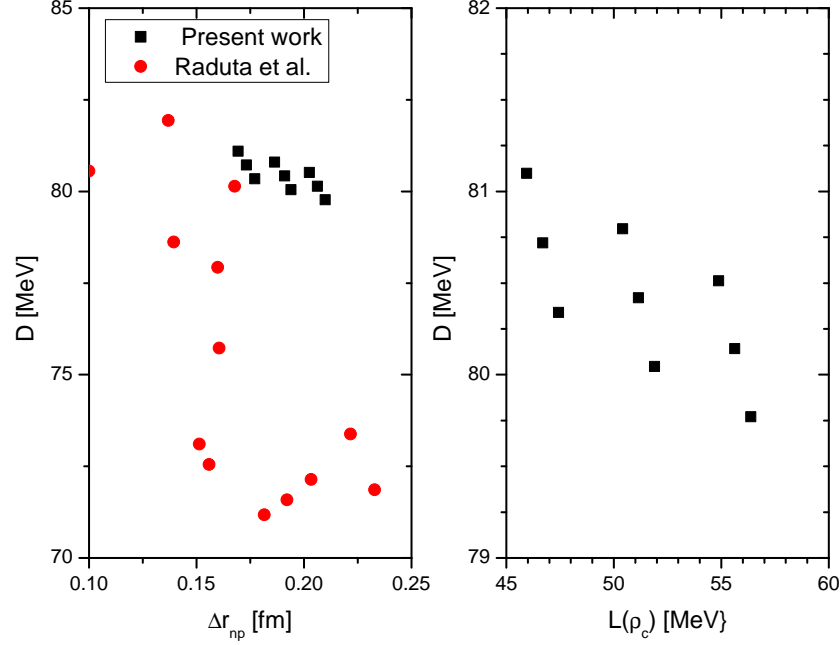


FIG. 16: (Left panel): The IVGDR energy in ^{208}Pb is plotted as a function of neutron skin thickness. The results of different Skyrme functionals are also shown in the figure. The correlation between these two quantities is very poor. (Right panel): The IVGDR energy is shown as a function of the density slope parameter at a reference density.

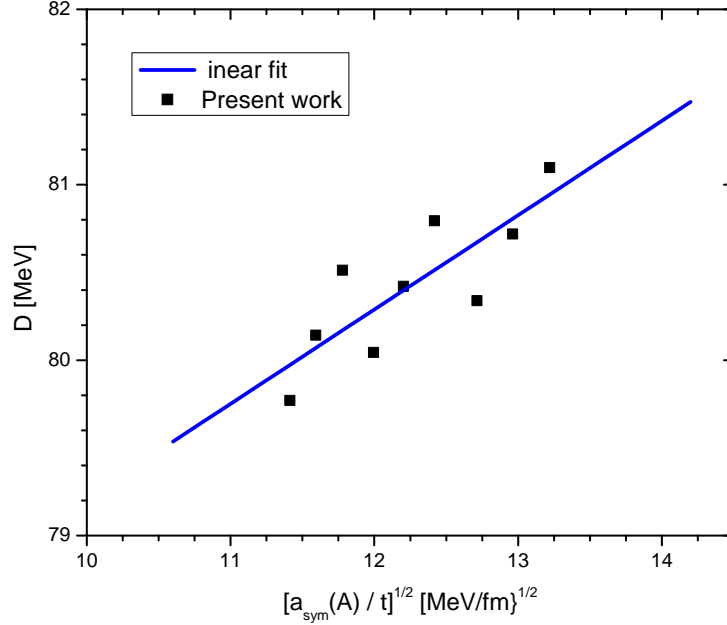


FIG. 17: The IVGDR energy is correlated with the quantity $\left(\frac{a_{sym}(A)}{t}\right)^{1/2}$.

work satisfactorily reproduce the properties of SNM at saturation density. We have considered the nuclear symmetry energy as saturation in the accepted range of 32 ± 2 MeV and obtained the density slope parameter in the range $44 \leq L(\rho_0) \leq 66$ MeV and the curvature parameter in the range $-201 \leq K_{sym} \leq -126$ MeV. These values are well within the constrained values from different analysis. The EoSs obtained in the present work not only satisfy the constraints for NSE in the subnormal densities but also pass within the experimentally extracted region of Russotto et al.[74]. The constraints coming from astrophysical and terrestrial laboratories limits the NSE at a

density twice the normal nuclear matter density as $E_s(2\rho_0) = 46.9 \pm 10.1 \text{ MeV}$ [69, 70]. The prediction for NSE from our EoSs lie well within these limits at $2\rho_0$ and therefore viable for different nuclear studies for a wide range of density domain. For the given range of $E_s(\rho_0)$ and $E_s(\rho_c)$, we have obtained the density slope parameter in the range $46.69 \leq L(\rho_c) \leq 55.63 \text{ MeV}$ and the curvature symmetry energy at a subsaturation density in the range $-120.69 \leq K_{sym} \leq -82.80 \text{ MeV}$. It is worth to mention here that while constraints on $L(\rho_c)$ are available in literature there are no reliable constraints on $K_{sym}(\rho_c)$. The predicted values of $L(\rho_c)$ are in conformity with the available constraints [14].

We have analysed the correlation of the neutron skin thickness in ^{208}Pb with different isovector parameters. In order to calculate the NST, we required the values of the symmetry coefficient $a_{sym}(A)$ as a function of mass number. We assumed the relationship $a_{sym}(A) \simeq E_s(\rho_A)$. It is worth to mention here that, this relation has already been verified by many workers for different mean field calculations. From the calculated values of $a_{sym}(A)$ we have extracted the values of surface symmetry energy in a leptodermous expansion. We could able to find a linear relationship between the surface symmetry energy contribution with the density slope parameter at a subsaturation density $L(\rho_c)$. The NST is calculated within the framework of droplet model using the finite range effective interaction. Instead of correlating the NST with the usual density slope parameter at saturation or the quantity $E_s(\rho_0) - a_{sym}(A)$, we find it reasonable to have a correlation between Δr_{np} with the isovector indicators such as $1 - \frac{a_{sym}(A)}{E_s(\rho_0)}$ and $\beta = \frac{E'_s(\rho_0)}{E_s(\rho_0)}$. Particularly, we emphasize upon the correlation between the bulk part of the NST with these quantities. We have obtained a strong correlation in the case of the bulk part of NST than the case of NST. The NST as predicted from our EoSs lies in the range $0.17 - 0.21 \text{ fm}$ with a spread of 0.04 fm . These values are in conformity with the experimentally extracted values of NST from different works. We have explored the correlation between the NST and its bulk part with the density slope parameter at a subsaturation density. A linear fit of Δr_{np} to the quantity $\beta' = \frac{L(\rho_c)}{3E_s(\rho_0)}$ is obtained from the correlation procedure. A similar correlation between the NST and the curvature symmetry parameter at subsaturation density is obtained from the calculation. We have tried to correlate the energy constant of IVGDR with $L(\rho_c)$ but found a poor correlation as compared to that of the neutron skin thickness case. However, an analytic linear dependence of the IVGDR energy constant with the quantity $\left(\frac{a_{sym}(A)}{t}\right)^{1/2}$ is obtained which may be useful for unleashing some uncertainty in the density dependence of nuclear symmetry energy.

References

- [1] B. A. Li, P. G. Krastev, D. H. Wen and N. B. Zhang, *Eur. Phys. J. A*, **55**, 217 (2019).
- [2] J. Lattimer and M. Prakash, *Phys. Rep.*, **333-334**, 121 (2000).
- [3] A. W. Steiner, M. Prakash, J. Lattimer, P. Ellis, *Phys. Rep.*, **41**, 325 (2005).
- [4] A. W. Steiner, S. Gandolfi, *Phys. Rev. Lett.*, **108**, 081102 (2012).
- [5] F. Ji, J. Hu, S. Bao and H. Shen, *Phys. Rev. C*, **100**, 045801 (2019).
- [6] J. Lattimer and M. Prakash, *Phys. Rep.*, **442**, 109 (2007).
- [7] T. Klahn, D. Blaske, S. Typel, E. N. E. Van Dalen, A. Faessler, C. Fuchs, T. Gaitanos, H. Grigorian, A. Ho, et al., *Phys. Rev. C*, **74**, 035802 (2006).
- [8] D. T. Loan, N. H. Tan, D. T. Khoa, J. Margueron, *Phys. Rev. C*, **83**, 065809 (2011).
- [9] M. B. Tsang, Y. Zhang, P. Danielewicz, M. Famiano, Z. Li, W. G. Lynch and A. W. Steiner, *Phys. Rev. Lett.*, **102**, 122701 (2009).
- [10] M. B. Tsang et al., *Phys. Rev. C* **86**, 015803 (2012).
- [11] J. Peikarewicz J et al., *Phys. Rev. C*, **85**, 041302(R) (2012).
- [12] A. Tamii, I. Poltoratska, P. von Neumann-Cosel, Y. Fujita, T. Adachi, C. A. Bertulani, J. Carter, M. Dozono, H. Fujita, K. Fujita et al., *Phys. Rev. Lett.*, **107**, 062502 (2011).
- [13] X. Roca-Maza, M. Brenna, G. Colo, M. Centelles, X. Vinas, B. K. Agrawal, N. Paar, D. Vretenar and J. Piekarewicz, *Phys. Rev. C*, **88**, 024316 (2013).
- [14] Z. Zhang and L. W. Chen, *Phys. Rev. C*, **90**, 064317 (2014).
- [15] S. Goriely, N. Chamel, J M Pearson, *Phys. Rev. Lett.*, **102**, 152503 (2009).
- [16] N. Wang, M. Liu, X. Z. Wu, J. Meng, *Phys. Lett. B*, **734**, 215 (2014).
- [17] J. L. Tian, H. T. Cui, K. K. Zheng, N. Wang *Phys. Rev. C*, **90**, 024313 (2014).
- [18] W. C. Chen, J. Peikarewicz, *Phys. Lett. B*, **748**, 284 (2015).
- [19] M. Warda, X. Vinas, X. Roca-Maza and M. Centelles, *Phys. Rev. C*, **80**, 024316 (2009).
- [20] X. Vinas, M. Centelles, X. Roca-Maza, and M. Warda, *Eur. Phys. J. A*, **50**, 27 (2014).
- [21] C. Mondal, B. K. Agrawal, M. Centelles, G. Colo, X. Roca-Maza, N. Paar, X. Vinas, S. K. Singh and S. K. Patra, *Phys. Rev. C*, **93**, 064303 (2016).
- [22] N. Wang, L. Ou, M. Liu, *Phys. Rev. C*, **87**, 034327 (2013).
- [23] Z. Zhang and L. W. Chen, *Phys. Lett. B*, **726**, 234 (2013).
- [24] B. K. Agrawal, J. N. De and S. K. Samaddar, *Phys. Rev. Lett.*, **94**, 032701 (2012).
- [25] B. K. Agrawal, J. N. De, S. K. Samaddar, S K, G. Colo, A. Sulaksono, *Phys. Rev. C*, **87**, 051306(R) (2013).
- [26] T. Hashimoto et al., *Phys. Rev. C*, **92**, 031305 (2015).
- [27] A. Tonchev, N. Tsoneva, C. Bhatia, A. Arnold, S. Goriely, et al. , *Phys. Lett. B*, **773**, 20 (2017).

- [28] A. Tamii, P. von Neumann Cosel and I. Poltoratska, *Eur. Phys. J. A*, **50**, 28 (2014).
- [29] P. Moller, W. D. Myers, H. Sagawa and S. Yoshida, *Phys. Rev. Lett.*, **108**, 052501(2012).
- [30] J. Dong, W. Zuo, J. Gu and U. Lombardo, *Phys. Rev. C*, **85**, 034308 (2012).
- [31] A. Trzcinska et al., *Phys. Rev. Lett.*, **87**, 082501 (2001).
- [32] B. A. Brown, G. Shen, G. C. Hillhouse, J. Meng and A. Trzcinska, *Phys. Rev. C*, **87**, 034305 (2007).
- [33] B. Klos et al., *Phys. Rev. C*, **76**, 014311 (2007).
- [34] J. Zenihiro, et al., *Phys. Rev. C*, **82**, 044611 (2010).
- [35] X. Roca-Maza, B. K. Agrawal, G. Colo, W. Nazarewicz, N. Paar, J. Piekarewicz, P. G. Reinhard and D. Vretenar, *AIP Conf. Proc.*, **1491**, 204 (2012).
- [36] PREX collaboration (S. Abrahamyan, Z. Ahmed et al.), *Phys. Rev. Lett.*, **108**, 112502 (2012).
- [37] W. D. Myers and W. J. Swiatecki, *Nucl. Phys. A*, **336**, 267 (1980).
- [38] M. Centelles, X. Roca-Maza, X. Vinas and M. Warda, *Phys. Rev. C*, **82**, 054314 (2010).
- [39] X. Roca-Maza, M. Centelles, X. Vinas, M. Warda, *Phys. Rev. Lett.*, **106**, 252501 (2011).
- [40] Y. Zhou and L. W. Chen, *Astrophys. J.*, **886**, 52 (2019).
- [41] G. F. Berstch, S. Dasgupta, *Phys. Rep.* **160**, 189 (1988).
- [42] W. A. Kuper, G. Wegman and E. R. Hilf, *Ann. Phys.(NY)* **88**, 454 (1974).
- [43] Q. Pan, P. Danielewicz, *Phys. Rev. Lett.*, **70**, 2062 (1993).
- [44] V. de La Mota, F. Seville, B. Remand, P. Schuk, *Phys. Rev. C* **46**, 667 (1992).
- [45] J. Zhang, S. Dasgupta, C. Gale, *Phys. Rev. C* **50**, 1617 (1994).
- [46] F. Haddad, F. Seville, M. Marine, V. de La Mota, P. Schuk, B. Johault, *Phys. Rev. C* **52**, 2013 (1995).
- [47] P. Danielewicz, *Phys. Rev. Lett.* **81**, 2438 (1998).
- [48] P. Danielewicz, *Nucl. Phys. A* **673**, 375 (2000).
- [49] T. R. Routray, B. Sahoo, R. K. Satpathy and B. Behera, *J. Phys. G: Nucl.Part. Phys.* **26**, 887 (2000).
- [50] B. Behera, T. R. Routray and R. K. Satpathy, *J. Phys. G: Nucl.Part. Phys.*, **24**, 2073 (1998).
- [51] B. Behera, T. R. Routray, B. Sahoo and R. K. Satpathy, *Nucl. Phys. A*, **609**, 770 (2002).
- [52] B. Behera, T. R. Routray and A. Pradhan, *Mod. Phys. Lett. A*, **20**, 2639 (2005).
- [53] B. Behera, T. R. Routray and S. K. Tripathy, *J. Phys. G: Nucl.Part. Phys.*, **36**, 125105 (2009).
- [54] B. Behera, T. R. Routray and S. K. Tripathy, *J. Phys. G: Nucl.Part. Phys.*, **38**, 115104 (2011).
- [55] T. R. Routray, S. K. Tripathy, B. B Dash, B. Behera and D. N. Basu, *Eur. Phys. J. A*, **47**, 92 (2011).
- [56] B. Behera, T. R. Routray, A. Pradhan, S. K. Patra and P. K. Sahu, *Nucl. Phys. A*, **794**, 132 (2009).
- [57] V. Baran, M. Colona, V. Greco and M. Di Toro, *Phys. Rep.* , **410**, 335 (2005).
- [58] B. A. Li, L. W. Chen and C. M. Ko, *Phys. Rep.* **464**, 113 (2008).
- [59] J. Lattimer, *Annu. Rev. Nucl. Part. Sci.* , **62**, 485 (2012).
- [60] C. J. Horowitz et al., *J. Phys. G: Nucl.Part. Phys.*, **41**, 093001 (2014).
- [61] M. Dutra, O. Lourenco, J. S. S. Martins, A. Delfino, J. R. Stone and P. D. Stevenson, *Phys. Rev. C*, **85**, 035201 (2012).
- [62] N. Wang, M. Liu, L. Ou and Y. Zhang, *Phys. Lett. B*, **751**, 553 (2015).
- [63] J. Lattimer and Y. Lim, *Astrophys. J.*, **771**, 51 (2013).
- [64] P. Danielewicz and J. Lee, *Nucl. Phys. A*, **818**, 36 (2009).
- [65] X. Roca-Maza, X. Vinas, M. Centelles, B. K. Agrawal, G. Colo, N. Paar, J. Piekarewicz and D. Vretenar, *Phys. Rev. C*, **92**, 064304 (2015).
- [66] D. M. Rossi, P. Adrich, F. Aksouh, H. Alvarez-Pol, T. Aumann, J. Benlliure, M. Bohmer, K. Boretzsky, E. Casarejos, M. Chartier et al., *Phys. Rev. Lett.*, **111**, 242503 (2013).
- [67] L. W. Chen, C. M. Ko, B. A. Li and J. Xu, *Phys. Rev. C*, **82**, 024321 (2010).
- [68] B. P. Abbott et al. (LIGO and VIRGO collaborations), *Phys. Rev. Lett.*, **121**, 161101 (2018).
- [69] N. B. Zhang and B. A. Li, *Eur. Phys. J. A*, **55**, 39 (2019).
- [70] B. A. Li, P. G. Krastev, D. H. Wen, W. J. Xie and N. B. Zhang, *AIP conference proceedings*, **2127**, 020018 (2019).
- [71] H. Tong, P. Zhao and J. Meng, *Phys. Rev. C*, **101**, 035802 (2020).
- [72] W. J. Xie and B. A. Li, arXiv: 1907.10741 (2019).
- [73] Y. Zhang, M. Liu, C. J. Xia, Z. Li and S. K. Biswal, *Phys. Rev. C*, **101**, 034303 (2020).
- [74] P. Russotto, S. Gannon et al., *Phys. Rev. C*, **94**, 034608 (2016).
- [75] P. Russotto et al., *Phys. Lett. B*, **697**, 471 (2011).
- [76] H. T. Cromartie, E. Fonseca, S. M. Ransom, et al., *NatAs*, doi:10.1038/s41550-019-0880-2, (2019).
- [77] J. M. Lattimer and A. W. Steiner, *Eur. Phys. J. A*, **50**, 40 (2014).
- [78] M. Centelles, X. Roca-Maza, X. Vinas and M. Warda, *Phys. Rev. Lett.*, **102**, 122502 (2009).
- [79] M. Brack, C. Guet and H. B. Hakansson, *Phys. Rep.*, **123**, 275 (1985).
- [80] M. Centelles, M. Del Estal and X. Vinas, *Nucl. Phys. A*, **635**, 193 (1998).
- [81] J. Treiner and H. Krivine, *Ann. Phys.*, **170**, 406 (1986).
- [82] L. W. Chen, arXiv:1101.5217 (2011).
- [83] E. Chabanat, P. Bonche, P. Haensel, J. Meyer and R. Schaeffer, *Nucl. Phys. A*, **635**, 231 (1998).
- [84] N. Wang, M. Liu, H. Jiang, J. L. Tian and Y. M. Zhao, *Phys. Rev. C*, **91**, 044308 (2015).
- [85] Ad. R. Raduta and F. Gulminelli, arXiv: 1712.05973 (20180).
- [86] Z. Zhang, Y. Lim, J. W. Holt and C. M. Ko, *Phys. Lett. B*, **777**, 73 (2018).
- [87] C. M. Tarbert et al. (Crystal Ball at MAMI and A2 Collaboration), *Phys. Rev. Lett.*, **112**, 242502 (2014).
- [88] J. P. Blocki, A. G. Magner, P. Ring and A. A. Vlasenko, *Phys. Rev. C*, **87**, 044304 (2013).